Discriminating between Metallic and Semiconducting Single-Walled Carbon Nanotubes Using Physisorbed Adsorbates: Role of Wavelike Charge-Density Fluctuations

Wang Gao, Yun Chen, and Qing Jiang*
Key Laboratory of Automobile Materials (Jilin University), Ministry of Education, Department of Materials Science and Engineering, Jilin University, Changchun 130022, China
(Received 24 April 2016; published 9 December 2016)

Discriminating between metallic (M) and semiconducting (S) single-walled carbon nanotubes (SWNTs) remains a fundamental challenge in the field of nanotechnology. We address this issue by studying the adsorption of the isotropic atoms Xe, Kr, and a highly anisotropic molecule n heptane on M- and S-SWNTs with density functional theory that includes many-body dispersion forces. We find that the distinct polarizabilities of M- and S-SWNTs exhibit significantly different physisorption properties, which are also strongly controlled by the SWNT's diameter, adsorption site, adsorbate coverage, and the adsorbate's anisotropy. These findings stem from the wavelike nature of charge-density fluctuations in SWNTs. Particularly, these results allow us to rationalize the unusual $\sqrt{3} \times \sqrt{3}R30^0$ phase of Kr atoms on small gap M-SWNTs and the double desorption peak temperatures of n heptane on M-SWNTs in experiments, and also propose the n heptane as an effective sensor for experimentally discriminating M- and S-SWNTs.

DOI: 10.1103/PhysRevLett.117.246101

The identification of metallic (M) and semiconducting (S) single-walled carbon nanotubes (SWNTs) plays a central role in the development of SWNT-based devices, since experimentally synthesized SWNTs are normally mixtures of M- and S-SWNTs rather than just one type as required for many applications. Although some pioneering methods have been useful in identifying the type of SWNTs [1–3], effective methods, using physisorbed adsorbates that do not damage SWNTs and distinguish M- and S-SWNTs effectively, are still urgently needed. Moreover, investigating the interactions between adsorbates and SWNTs is crucial for many additional applications, e.g., quantum devices and hydrogen storage [4,5]. As the primary driving force behind physisorption, van der Waals (vdW) forces exhibit different asymptotic behaviors depending on the range scale of electronic fluctuations [6–12]. Hence, unraveling the physisorption of M- and S-SWNTs is of great importance for understanding the fundamental nature of vdW forces, as well as for accelerating applications of SWNTs [13–15].

M-SWNTs possess infinite static longitudinal polarizabilities, whereas S-SWNTs have finite longitudinal polarizabilities [16]. Generally, this difference is expected to result in significantly different physisorption [14,17–21]. Dobson *et al.* [9] fulfilled this expectation in conducting and nonconducting wires via random-phase approximation (RPA), but did not explore the interactions between adsorbates and wires. RPA is also prone to underestimating intermolecular vdW forces [22]. A pairwise method by Rajter *et al.* [23] and a quantum electrodynamical approach by Popescu *et al.* [24] yielded conflicting priority for the interactions between S-SWNTs and those between M-SWNTs. In addition, both studies did not address the interactions between adsorbates and SWNTs. Using a coupled dipole method, Kim *et al.* [25] and Shtogun *et al.* [26] reported the importance of many-body vdW forces for linear and graphitic nanoclusters. With a nonlocal many-body dispersion method (MBD) [27,28], Ambrosetti *et al.* demonstrated that wavelike charge-density fluctuations are responsible for the MBD forces between infinite S-SWNTs [8]. However, the physisorption difference between M- and S-SWNTs was not clarified.

Through a combination of temperature-programed desorption (TPD) measurements and vdW-corrected density functional theory (DFT) calculations, Chen *et al.* [29,30] indicated a negligible difference between the adsorption energies for isotropic atom Xe and highly anisotropic n heptane on M- and S-SWNTs, despite their significantly different polarizabilities. Indeed, the TPD measurements obtained only identical desorption peak temperatures on M- and S-SWNTs [29,30]. The corresponding adsorption energies were estimated by assuming the same preexponential factor ν in the Redhead equation [31] for both M- and S-SWNTs. However, the preexponential factor ν depends strongly on the size of adsorbed molecules and the identity of the SWNT [32], and deviates significantly between different measurements (10^{17}–10^{19} s^{-1} for n heptane desorbing on graphite) [33–36]. This can result in significant uncertainties in the adsorption energies. The application of DFT + TS (Tkatchenko-Scheffler vdW scheme) [37] and vdW-DF2 methods [38] is inappropriate because they cannot correctly capture the MBD forces that stem from the nonlocal anisotropic polarization of SWNTs, and thus are incapable of correctly describing physisorption on SWNTs. In particular, these methods failed to reproduce the unusual $\sqrt{3} \times \sqrt{3}R30^0$ phase of Kr on graphite and SWNTs (named

as the triangular 1/6 phase), yielding much higher density phases than those observed in experiments [39]. This failure has been attributed to underestimation of corrugation effects on SWNTs [40,41].

In this Letter, we revisit the adsorption of isotropic atoms Xe, Kr, and a highly anisotropic molecule *n* heptane on *M*- and *S*-SWNTs, by using a DFT method that includes nonlocal MBD forces (DFT + MBD) [27,28]. We find that the wavelike fluctuations of charge density primarily determine the physisorption properties of SWNTs. Thus, the distinct polarizabilities of *M*- and *S*-SWNTs lead to the distinct adsorption properties, which also depend strongly on the SWNT's diameter, adsorption site, adsorbate coverage, and the anisotropy of the adsorbate. We are able to identify the triangular 1/6 phase on a small gap *M*-SWNT, which is in reasonable agreement with experiments [39]. On the basis of the strikingly different adsorption properties for *n* heptane on *M*- and *S*-SWNTs, we provide a potential solution for distinguishing between *M*- and *S*-SWNTs.

All calculations were performed by using the FHI-aims code with a "tight" basis set [42]. Eight different SWNTs with the diameters of 7.8–16.2 Å (the usual diameters of SWNTs are 4–20 Å [43]), four metallic [(n, n)] and four semiconducting [$(n, 0)$ with $n \neq 3m$], were adopted and divided into four groups, each of which consisted of one *M*-SWNT and one *S*-SWNT with almost the same diameter. We obtained the geometric and energetic details using Perdew-Burke-Ernzerhof (PBE) [44] augmented with the TS and MBD methods (PBE + TS and PBE + MBD). Neither MBD nor pairwise vdW approximations like TS are able to explicitly capture the free-electron response. However, free electrons are responsible for only a tiny fraction of the entire response in SWNTs and only become important at very low frequencies, whereas the vdW energy comes from integration from zero to infinite frequencies. Previous studies have demonstrated that MBD can accurately treat delocalized π systems such as graphene/*h*-BN and describe the vdW coefficients of nanotubes [11,45], while such effects are missed by pairwise schemes of vdW interactions. We used a vacuum width of 100 Å to separate periodic images and a *k*-point grid of $1 \times 1 \times 4$ for a $1 \times 1 \times 2$ supercell of *S*-SWNT and a $1 \times 1 \times 3$ supercell of *M*-SWNT, both of which converge adsorption energies to an meV/atom level.

We calculated the binding curves of Xe adsorption outside and inside the four grouped SWNTs and summarize the results in Fig. 1 (Fig. S1 and Table SI of the Supplemental Material [46]). PBE + TS predicts that the adsorption energy of Xe on *M*-SWNTs is nearly identical to that on *S*-SWNTs in each group (with the deviation < 2%), which is consistent with literature results using vdW-DF2 and PBE + TS [29,30]. In stark contrast, PBE + MBD demonstrates that the adsorption energy of Xe is up to 87.5% larger on *M*-SWNTs than on *S*-SWNTs, explicitly demonstrating that the distinct longitudinal polarizabilities lead to the significantly different physisorption properties of the SWNTs.

The absolute MBD adsorption energies are less than 50% of the TS ones, whereas the MBD adsorption energies for Xe on *M*-SWNTs deviate from those of Xe on *S*-SWNTs by 8.1%–56.1% (Fig. S1 and Table SI in the Supplemental Material [46]). The former results from the many-body effects of vdW forces, which stem from the highly nonlocal anisotropic polarization of SWNTs. The later reflects the distinct vdW forces derived by the distinct polarizabilities of *M*- and *S*-SWNTs.

To uncover the mechanism behind this phenomenon, we investigated the collective charge-density fluctuations

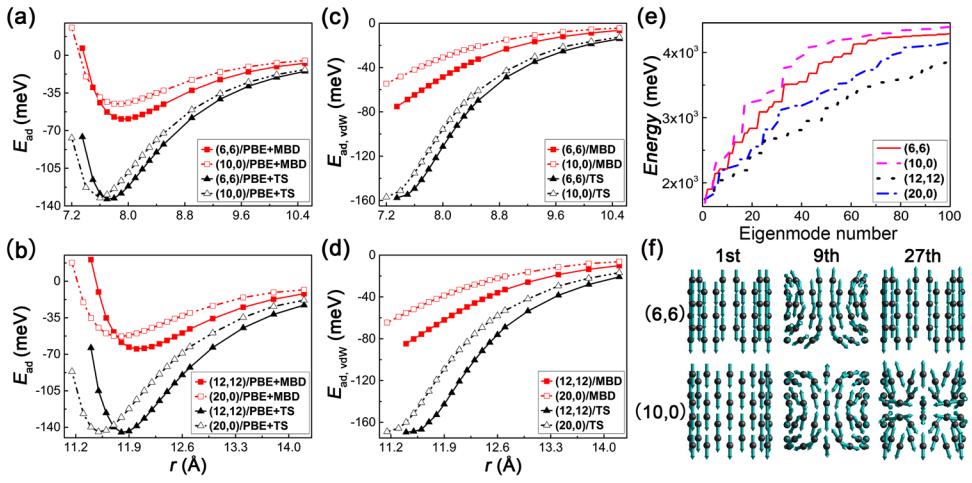

FIG. 1. Adsorption potential energies by PBE + MBD and PBE + TS (MBD and TS) for Xe adsorption at the outside sites of $(6, 6)/(10, 0)$ SWNTs (a) [(c)] and of $(12, 12)/(20, 0)$ SWNTs (b) [(d)], as a function of the distance, *r* in Å, from the axis of the specific SWNT. (e) MBD eigenvalue spectrum for the above SWNTs that is the $3N$ collective eigenmodes by the MBD model in ascending order (shown until the energy of 4900 meV), along with (f) schematic illustration of several representative (1st, 9th, and 27th) low-energy collective MBD eigenmodes in (e).

of the two groups of SWNTs by plotting the MBD eigenvalue spectrum and collective MBD eigenmodes in Figs. 1(e)–1(f). In each group of SWNTs, the M-SWNT has a lower energy compared with the S-SWNT for each collective MBD eigenmode at the low-energy range of the spectrum. It is known that the static dipole polarizability α is correlated with the resonant frequency of the ith eigenmode ω_i by the constant quantity $\alpha\omega_i^2$ for every MBD eigenmode, due to charge conservation [8]. Compared with S-SWNTs, the lower-energy eigenmodes of M-SWNTs correspond to higher polarizabilities, indicating more delocalized charge-density fluctuations over the entire SWNT and stronger dipole-dipole coupling along the longitudinal axis of SWNTs [Fig. 1(f)]. In contrast, the higher-energy eigenmodes have increasing transverse components. Since the lower-energy longitudinal eigenmodes dominate over transverse eigenmodes in determining the interactions between SWNTs and Xe, the M-SWNTs exhibit more pronounced MBD binding energies than the S-SWNTs.

It is apparent that the distinct vdW forces of M- and S-SWNTs can only be described correctly using the wavelike charge-density fluctuations of SWNTs (MBD), rather than with particlelike or fragmentlike dipolar fluctuations (pairwise schemes such as TS and vdW-DF2).

The many-body effects of vdW forces also modify the adsorption geometries for Xe on SWNTs. PBE + MBD generates similar adsorption distances of $d = 3.8$–4 Å for all the cases considered, which is consistent with the sum of the vdW radii of C and Xe atoms ($1.7 + 2.16 = 3.86$ Å) [47]. In contrast, PBE + TS generally yields adsorption distances that are shorter than PBE + MBD (by 0.1–0.3 Å) because TS overestimates the vdW forces. The only exception is adsorption inside $(6,6)/(10,0)$, where optimal position of Xe is exactly at the center of the SWNTs with PBE + TS, but is $r = 0.1$ Å away from the center of the SWNTs with PBE + MBD. This difference is due to the different trends exhibited by the binding curves for TS (binding energy decreases with increasing r) and MBD (binding energy increases with increasing r) (Fig. S2 of the Supplemental Material [46]). Because the PBE binding energy decreases with increasing r, the competition between the PBE and MBD energies leads to the optimal position of Xe at $r = 0.1$ Å inside $(6,6)/(10,0)$. The corresponding energetic gains are 3 meV for (6, 6) and 1 meV for (10, 0) relative to the center of the SWNTs.

To unravel the optimal commensurate solid phase (CS) of adsorbed Kr atoms on SWNTs, we used PBE + MBD to study three possible types of CS phases on zigzag M-SWNTs $(n, 0)$ with $n = 3m$ including the striped $1/4$ phase, the triangular $1/4$ phase, and the triangular $1/6$ phase as a function of the index n [Figs. 2(a), 2(b)]. We found that the relative stability of these three phases is determined by the SWNT's diameter: the striped $1/4$ phase is the most stable one for $n \leq 12$, the triangular $1/4$ phase for $12 < n \leq 24$, and the triangular $1/6$ phase for $n > 24$. Thus, the (27, 0) with a diameter of $D = 21.14$ Å is the narrowest small gap M-SWNT that favors the triangular $1/6$ phase. This nanotube is much narrower than those obtained by the classical grand canonical Monte Carlo (GCMC) simulations and vdW-DF2 methods ($D \geq 31.34$ Å) [30,48], and is thus in better agreement with experimental observations ($D = 10$–30 Å) [39].

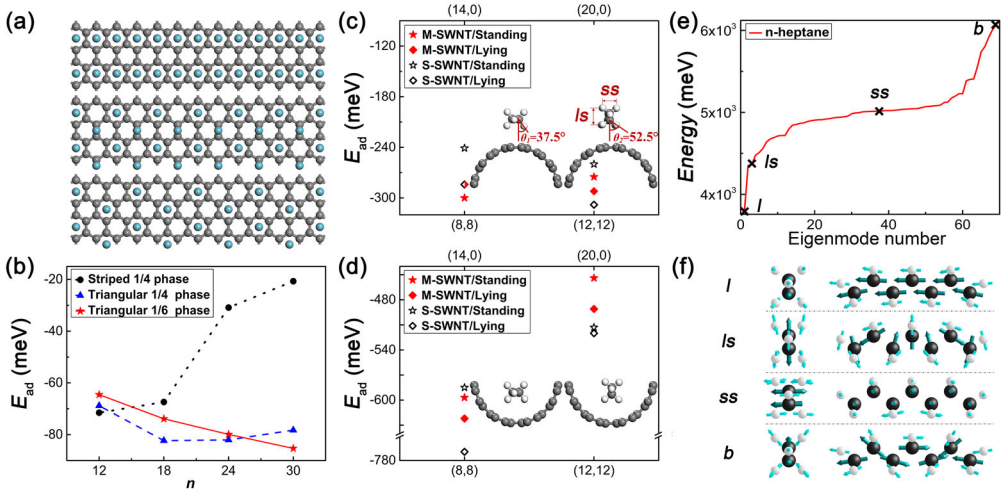

FIG. 2. (a) 2D schematic illustration of three Kr CS phases by "unrolling" the cylindrical structures of SWNTs. From top to bottom: the striped $1/4$ phase, the triangular $1/4$ phase, and the triangular $1/6$ phase (Kr atoms in blue). (b) Comparison of adsorption energies per Kr atom (by PBE + MBD) of the three Kr CS phases on zigzag M-SWNTs, as a function of the index n. (c) [(d)] Adsorption energies by PBE + MBD corresponding to n heptane lying or standing outside [inside] $(8,8)/(14,0)$ and $(12,12)/(20,0)$, respectively. (e) MBD eigenvalue spectrum for n heptane that is the $3N$ collective eigenmodes by the MBD model in ascending order. (f) Schematic illustration of representative collective MBD eigenmodes for n heptane [l, ls, ss, and b as indicated in (e)] with both front and side views.

Our results demonstrate that, in addition to the anisotropy of SWNTs proposed by the studies of empirical anisotropic potentials [40,41], the coverage- and size-dependent properties of the Kr-Kr interactions are also critical for the formation of the triangular 1/6 phase. We separated the total adsorption energy of the Kr phases on SWNTs into the Kr-Kr interaction energy and the Kr phases-SWNTs interaction energy ($E_{\mathrm{tot}} = E_{\mathrm{Kr-Kr}} + E_{\mathrm{Krp-S}}$, Table I). On (18,0), the many-body effects of the vdW forces (which are difference between PBE + MBD and PBE + TS) for $E_{\mathrm{Kr-Kr}}$, which depend strongly on the Kr coverage and favor the triangular 1/6 phase by 9 meV/atom relative to the triangular 1/4 phase, are, unfortunately, missed in GCMC and vdW-DF2 simulations [30,48]. As the index n of $(n, 0)$ is increased from 12 to 30, $E_{\mathrm{Kr-Kr}}$ is always attractive for the triangular 1/6 phase ($d_{\mathrm{Kr-Kr}}$ decreases from 6.69 to 5.25 Å), but for the triangular 1/4 phase is only attractive up to (24, 0) with $d_{\mathrm{Kr-Kr}} = 4.02$ Å and then becomes repulsive ($d_{\mathrm{Kr-Kr}}$ decreases from 4.89 to 3.87 Å), because the binding distance of a Kr dimer is 4.04 Å [49]. Therefore, the triangular 1/6 phase becomes more stable than the triangular 1/4 phase on (27, 0). Clearly, describing $E_{\mathrm{Kr-Kr}}$ and $E_{\mathrm{Krp-S}}$ on equal footing is crucial for determining the Kr CS phases on SWNTs.

We further studied the adsorption of n heptane on two sets of SWNTs: $(8,8)/(14,0)$ and $(12,12)/(20,0)$. The side view of n heptane is not square but rectangular, with long-side and short-side directions (ls and ss) that lead to lying and standing adsorption configurations on the SWNTs [see Figs. 2(c), 2(d), in which the angle is defined relative to the vertical line]. PBE + TS yields nearly identical adsorption energies for each set of the SWNTs [30], with the same lying configuration. In contrast, PBE + MBD predicts not only different adsorption energies but also substantially different adsorption structures for n heptane on M- and S-SWNTs [Figs. 2(c), 2(d) and Table SII of the Supplemental Material [46]]: at the exterior sites of SWNTs, n heptane lies on S-SWNTs but can adopt either a lying or a standing configuration on M-SWNTs. Remarkably, this observation corresponds with the TPD experiments, in which the desorption of n heptane at the exterior sites generates a single peak temperature (199 K) on S-SWNTs but a pair of neighboring peaks (197 and 187 K) on M-SWNTs [30]. Experiments with infrared adsorption (IR) spectroscopy and scanning tunneling microscope (STM) should be able to identify and discern these lying and standing configurations, and thereby differentiate M- from S-SWNTs. We thus expect that n heptane can serve as a sensor for experimentally discriminating between M- and S-SWNTs.

TABLE I. Differences of the individual contributions ($E_{\mathrm{Kr-Kr}}$ and $E_{\mathrm{Krp-S}}$) and the corresponding total adsorption energies (E_{tot}) between triangular 1/6 phase and triangular 1/4 phase for Kr in meV per atom on (18, 0), by PBE + MBD (PBE + TS) and GCMC simulations with anisotropic (isotropic) Krp-S potential.

	$E_{1/6}$—$E_{1/4}$		
Method	$E_{\mathrm{Kr-Kr}}$	$E_{\mathrm{Krp-S}}$	E_{tot}
PBE + MBD (PBE + TS)	18.3 (27.3)	−9.9 (−11.8)	8.4 (15.5)
GCMC-aniso (iso) [48]	282 (276)	−61 (−15)	221 (261)

We have also analyzed the MBD adsorption energies of n heptane on SWNTs (Table SII), finding that the n-heptane anisotropy plays a crucial role in binding itself to SWNTs, which significantly differs from the isotropic Xe atoms and the linear one-dimensional carbynelike atomic wire [8]. As shown in Figs. 2(e) and 2(f), an increase of n heptane's eigenmodes energy is accompanied with an increase transverse components of eigenmodes, with charge-density fluctuations gradually changing from the longitudinal (l) direction to the C-H bond (b) direction through the ls and ss directions. The adsorption of n heptane on SWNTs is determined mainly by the eigenmodes of n heptane (represented by l, ls, ss, and b) and the corresponding eigenmodes of SWNTs (see Fig. S3 of the Supplemental Material [46]). At the outside sites of SWNTs, except the coupling between the l eigenmodes of n heptane and SWNTs, the lying n heptane has lower-energy ls eigenmodes contributing to its binding with SWNTs by coupling with the transverse components of SWNTs eigenmodes (e.g., the 5th eigenmode of the SWNT along the nanotube wall in Fig. S3 of the Supplemental Material [46]), whereas the standing n heptane has the ss eigenmodes doing so. Therefore, when adsorbed outside the SWNTs, n heptane has a larger MBD adsorption energy in the lying configuration than in the standing configuration. Compared with S-SWNTs, M-SWNTs have fewer transverse components of eigenmodes, leading to smaller differences in MBD adsorption energies between the lying and standing n heptane. The anisotropy of n heptane is thus vital to its adsorption properties on the outside of SWNTs. Inside SWNTs, the l eigenmodes of n heptane on M-SWNTs generate larger MBD adsorption energies than those on S-SWNTs, whereas ls, ss, and b of n heptane on S-SWNTs contribute to the MBD adsorption energies more than those on M-SWNTs, due to there being more transverse components in the S-SWNT eigenmodes. Since the resulting MBD adsorption energies are larger on S-SWNTs than on M-SWNTs, the n-heptane transverse eigenmodes, which result from its anisotropy, should thus be critical for its adsorption inside SWNTs.

In conclusion, our PBE + MBD calculations reveal the nature of the vdW forces in M- and S-SWNTs, which are governed by the wavelike charge-density fluctuations in SWNTs. We found that M- and S-SWNTs exhibit substantially different physisorption properties, which also depend strongly on the SWNT's diameter, adsorption site, adsorbate coverage, and the anisotropy of adsorbate. These

results allow us to explain experimental observations of the unique triangular 1/6 phase for Kr atoms on small gap *M*-SWNTs and the double desorption peaks for *n* heptane on *M*-SWNTs in TPD experiments. Moreover, the dramatic difference between the adsorption of *n* heptane on *M*- and *S*-SWNTs suggests a remarkable way for experimentally discriminating between *M*- and *S*-SWNTs, which could be helpful for the practical application of SWNTs. These results demonstrate that MBD interactions are essential for studying highly anisotropic nanomaterials.

We gratefully acknowledge support from the Program for the Thousand Young Talents Plan, New Century Excellent Talents in University (No. NCET-13-0255), the National Natural Science Foundation of China (No. 21673095, 51631004), and the computing resources of the High Performance Computing Center of Jilin University, and National Supercomputing Center in Jinan China.

W. G. and Y. C. contributed equally to this work.

*jiangq@jlu.edu.cn

[1] A. Bachtold, M. S. Fuhrer, S. Plyasunov, M. Forero, E. H. Anderson, A. Zettl, and P. L. McEuen, Phys. Rev. Lett. **84**, 6082 (2000).
[2] A. Jorio, R. Saito, J. H. Hafner, C. M. Lieber, M. Hunter, T. McClure, G. Dresselhaus, and M. S. Dresselhaus, Phys. Rev. Lett. **86**, 1118 (2001).
[3] R. Martel, T. Schmidt, H. R. Shea, T. Hertel, and P. Avouris, Appl. Phys. Lett. **73**, 2447 (1998).
[4] J. Schmiedmayer, R. Folman, and T. Calarco, J. Mod. Opt. **49**, 1375 (2002).
[5] A. C. Dillon, K. M. Jones, T. A. Bekkedahl, C. H. Kiang, D. S. Bethune, and M. J. Heben, Nature (London) **386**, 377 (1997).
[6] V. A. Parsegian, *Van der Waals Forces: A Handbook for Biologists, Chemists, Engineers, and Physicists* (Cambridge University Press, Cambridge, England, 2005).
[7] A. Tkatchenko, Adv. Funct. Mater. **25**, 2054 (2015).
[8] A. Ambrosetti, N. Ferri, R. A. DiStasio, and A. Tkatchenko, Science **351**, 1171 (2016).
[9] J. F. Dobson, A. White, and A. Rubio, Phys. Rev. Lett. **96**, 073201 (2006).
[10] A. Ruzsinszky, J. P. Perdew, J. Tao, G. I. Csonka, and J. M. Pitarke, Phys. Rev. Lett. **109**, 233203 (2012).
[11] V. V. Gobre and A. Tkatchenko, Nat. Commun. **4**, 2341 (2013).
[12] A. J. Misquitta, J. Spencer, A. J. Stone, and A. Alavi, Phys. Rev. B **82**, 075312 (2010).
[13] K. H. An, J. S. Park, C.-M. Yang, S. Y. Jeong, S. C. Lim, C. Kang, J.-H. Son, M. S. Jeong, and Y. H. Lee, J. Am. Chem. Soc. **127**, 5196 (2005).
[14] R. Krupke, F. Hennrich, H. v. Löhneysen, and M. M. Kappes, Science **301**, 344 (2003).
[15] W. Yang, K. R. Ratinac, S. P. Ringer, P. Thordarson, J. J. Gooding, and F. Braet, Angew. Chem., Int. Ed. Engl. **49**, 2114 (2010).
[16] B. Kozinsky and N. Marzari, Phys. Rev. Lett. **96**, 166801 (2006).
[17] D. Chattopadhyay, I. Galeska, and F. Papadimitrakopoulos, J. Am. Chem. Soc. **125**, 3370 (2003).
[18] M. Zheng, A. Jagota, E. D. Semke, B. A. Diner, R. S. McLean, S. R. Lustig, R. E. Richardson, and N. G. Tassi, Nat. Mater. **2**, 338 (2003).
[19] J. Lu, S. Nagase, X. Zhang, D. Wang, M. Ni, Y. Maeda, T. Wakahara, T. Nakahodo, T. Tsuchiya, T. Akasaka *et al.*, J. Am. Chem. Soc. **128**, 5114 (2006).
[20] T. Tanaka, H. Jin, Y. Miyata, S. Fujii, H. Suga, Y. Naitoh, T. Minari, T. Miyadera, K. Tsukagoshi, and H. Kataura, Nano Lett. **9**, 1497 (2009).
[21] P. Anilkumar, K. A. S. Fernando, L. Cao, F. Lu, F. Yang, W. Song, S. Sahu, H. Qian, T. J. Thorne, A. Anderson *et al.*, J. Phys. Chem. C **115**, 11010 (2011).
[22] X. Ren, A. Tkatchenko, P. Rinke, and M. Scheffler, Phys. Rev. Lett. **106**, 153003 (2011).
[23] R. F. Rajter, R. Podgornik, V. A. Parsegian, R. H. French, and W. Y. Ching, Phys. Rev. B **76**, 045417 (2007).
[24] A. Popescu, L. M. Woods, and I. V. Bondarev, Phys. Rev. B **83**, 081406 (2011).
[25] H.-Y. Kim, J. O. Sofo, D. Velegol, M. W. Cole, and A. A. Lucas, J. Chem. Phys. **124**, 074504 (2006).
[26] Y. V. Shtogun and L. M. Woods, J. Phys. Chem. Lett. **1**, 1356 (2010).
[27] A. Tkatchenko, R. A. DiStasio, Jr., R. Car, and M. Scheffler, Phys. Rev. Lett. **108**, 236402 (2012).
[28] A. Ambrosetti, A. M. Reilly, R. A. DiStasio, Jr., and A. Tkatchenko, J. Chem. Phys. **140**, 18A508 (2014).
[29] D.-L. Chen, L. Mandeltort, W. A. Saidi, J. T. Yates, Jr., M. W. Cole, and J. K. Johnson, Phys. Rev. Lett. **110**, 135503 (2013).
[30] L. Mandeltort, D.-L. Chen, W. A. Saidi, J. K. Johnson, M. W. Cole, and J. T. Yates, Jr., J. Am. Chem. Soc. **135**, 7768 (2013).
[31] P. A. Redhead, Vacuum **12**, 203 (1962).
[32] J. B. Miller, H. R. Siddiqui, S. M. Gates, J. N. Russell, Jr., J. T. Yates, Jr., J. C. Tully, and M. J. Cardillo, J. Chem. Phys. **87**, 6725 (1987).
[33] K. E. Becker and K. A. Fichthorn, J. Chem. Phys. **125**, 184706 (2006).
[34] A. J. Gellman and K. R. Paserba, J. Phys. Chem. B **106**, 13231 (2002).
[35] S. L. Tait, Z. Dohnálek, C. T. Campbell, and B. D. Kay, J. Chem. Phys. **125**, 234308 (2006).
[36] K. R. Paserba and A. J. Gellman, Phys. Rev. Lett. **86**, 4338 (2001).
[37] A. Tkatchenko and M. Scheffler, Phys. Rev. Lett. **102**, 073005 (2009).
[38] K. Lee, É. D. Murray, L. Kong, B. I. Lundqvist, and D. C. Langreth, Phys. Rev. B **82**, 081101 (2010).
[39] Z. Wang, J. Wei, P. Morse, J. G. Dash, O. E. Vilches, and D. H. Cobden, Science **327**, 552 (2010).
[40] G. Vidali and M. W. Cole, Phys. Rev. B **29**, 6736 (1984).
[41] N. D. Shrimpton and W. A. Steele, Phys. Rev. B **44**, 3297 (1991).
[42] V. Blum, R. Gehrke, F. Hanke, P. Havu, V. Havu, X. Ren, K. Reuter, and M. Scheffler, Comput. Phys. Commun. **180**, 2175 (2009).
[43] L. Mleczko and G. Lolli, Angew. Chem., Int. Ed. Engl. **52**, 9372 (2013).

[44] J. P. Perdew, K. Burke, and M. Ernzerhof, Phys. Rev. Lett. **77**, 3865 (1996).
[45] W. Gao and A. Tkatchenko, Phys. Rev. Lett. **114**, 096101 (2015).
[46] See Supplemental Material at http://link.aps.org/supplemental/10.1103/PhysRevLett.117.246101 for the calculation details and the detailed data of adsorption of Xe and *n*-heptane inside and outside SWNTs.
[47] A. Bondi, J. Phys. Chem. **68**, 441 (1964).
[48] H.-Y. Kim, M. W. Cole, M. Mbaye, and S. M. Gatica, J. Phys. Chem. A **115**, 7249 (2011).
[49] A. K. Dham, A. R. Allnatt, W. J. Meath, and R. A. Aziz, Mol. Phys. **67**, 1291 (1989).